High temperature dislocation glide in the MoNbTi refractory multiprincipal element alloy

Morgan R. Jones, Lauren T. W. Fey, and Irene J. Beyerlein

Phys. Rev. Materials **8**, 013604 — Published 18 January 2024

DOI: 10.1103/PhysRevMaterials.8.013604

High temperature dislocation glide in the MoNbTi Refractory Multi-Principal Element Alloy

Morgan R. Jones[1*], Lauren T. W. Fey[1], Irene J. Beyerlein[1,2]

[1] *Materials Department*
University of California Santa Barbara
Santa Barbara, CA, USA

[2] *Department of Mechanical Engineering*
University of California Santa Barbara
Santa Barbara, CA, USA

**Corresponding author*
morgan_jones@ucsb.edu

Abstract

Numerous body-centered cubic (bcc) refractory multi-principal element alloys (RMPEAs) exhibit high-temperature strengths that surpass those of Ni-based superalloys. The superior properties of RMPEAs have been shown to stem in part from the unique dislocation glide mechanisms in compositionally disordered systems. Here, using a three-dimensional phase field dislocation dynamics approach combined with Langevin dynamics, we simulate the glide mechanisms of screw and edge dislocations at elevated temperature and low stress levels in the RMPEA MoNbTi with a body centered cubic, random solid solution structure. For 600K−1200K, edge dislocation glide is smooth, temperature sensitive, and faster than screw dislocation glide. Screw dislocations exhibit three distinct glide mechanisms over the same temperature range. Ultimately, the formation of nonplanar kink pairs that ensues above 900K reduces screw mobility with respect to temperature and leads to athermal mobility from 1100K−1200K.

Keywords: screw, edge, kink-pair, mobility, cross-slip

Introduction

A set of advanced alloys known as refractory multi-principal element alloys (RMPEAs) have received intense interest in the scientific community due to a range of exceptional material properties, including high yield strength at elevated temperature, corrosion/erosion resistance, radiation resistance, and creep resistance [1,2]. Many believe that body-centered cubic (bcc) RMPEAs are the key to replacing components made from traditional alloys (e.g., face centered cubic (fcc) Ni-based superalloys), which are currently the limiting factor in achieving higher thermal efficiency [1,3]. Uncovering the mechanistic origins of their high strength can provide meaningful routes to the discovery and design of RMPEAs [4–7]. RMPEAs are distinguished from traditional alloys by their composition. They comprise three or more primarily refractory elements in similar portions [2]. This compositional disorder leads to an atomic and nanoscale complexity that warrants revisiting the microscopic mechanisms, such as dislocation motion, that determine strength [1,2,8,9]. Since their introduction, numerous studies have been dedicated to better understand RMPEA microstructure and deformation response over a wide range of compositions and conditions and the dislocations that govern them [5,7,10–14]. However, fundamental studies

on dislocation glide mechanisms and motion at the high temperatures in the target applications are lacking [2,13,15,16].

One attractive feature of *some* RMPEAs that further motivates the need to understand elementary dislocation glide processes at high temperature is the so called "strength plateau". The yield strength of RMPEAs, such as MoNbTi, MoNbTaW, and MoNbTaVW, vary negligibly over the temperature range $T \cong 0.3T_{melt} - 0.5T_{melt}$ [5,17]. This property is distinctly different from the strength of traditional refractory alloys, which universally reduces over this same temperature range [18]. The prevailing notion is that the strength plateau can be attributed to unusual dislocation behavior, but very few studies have been dedicated to uncovering the specific mechanisms at play [15,16,19]. The end of the plateau is marked by a significant reduction in strength, which has been attributed to a transition from dislocation-controlled to a creep-controlled behavior [20–22].

Most RMPEAs have a body centered cubic (bcc) crystal structure. Studies of dislocation behavior in bcc materials come with the question of screw/edge dislocation character. It is widely accepted that the motion of screw-character dislocations at low homologous temperatures is the rate controlling mechanism, and as temperature increases, it is thought is that both screw- and edge-character dislocations participate [23–26]. In RMPEAs, however, their individual contributions to deformation at room temperature are unclear, and even more elusive at high temperatures. Experimental investigations on RMPEAs have shown mixed results on the dislocation types responsible for their high temperature strength. *In-situ* neutron diffraction and postmortem TEM characterization of deformed NbTaTiV specimens suggested that edge dislocation motion dominated at elevated temperatures [27]. Further, an in-situ TEM study on MoNbTi found that even at low temperatures, a large portion of the mobile dislocations were mixed-character (i.e., both types) dislocations [5]. Conversely, two separate postmortem TEM studies on deformed HfNbTaTiZr specimens at room temperature provided evidence pointing to screw dislocation-controlled deformation [28,29]. After deformation at elevated temperatures, a postmortem TEM analysis of NbTiZr concluded control by screw dislocations [16].

In recent years, several analytical and phenomenological dislocation-based models for the temperature-strength relationships of RMPEAs have been developed [7,21,22,30]. Among them, no consensus has been reached on which dislocation type dominates plasticity. Edge dislocation based analytical models have been successful in reproducing the temperature-strength relationships of some RMPEAs (e.g., NbTaTiV and CrMoNbV) up to 1900K, while proving unsuccessful for others (e.g., MoNbTaTi, NbTiZr, and HfNbTaTiZr) [7]. For RMPEAs, like MoNbTaTi, NbTiZr, and HfNbTaTiZr, a screw-based analytical model was found to capture the strength-temperature relationships more accurately [21]. None of these provided a mechanism to predict the strength plateau. An analytical edge-dislocation based model demonstrated that calculated yield strengths followed experimental yield strengths if the rate controlling dislocation type changed from screw to edge at the first strength plateau temperature [7]. A recent study reported on the impressively high and broad strength plateau of HfMoNbTaW and provided an accompanying Arrhenius-based model for screw and edge motion that supports the argument that the plateau results from a transition from screw to edge dislocation activity [19]. Enabling an analytical solution to fit well with experimental data, however, often involves adjustments or

parameters that are not explained based on mechanisms. Thus, there is still the question whether the physical picture posed from analytical models portrays actual dislocation glide processes.

A feasible route to systematically identifying dislocation glide mechanisms in RMPEAs is to simulate dislocation motion under mechanical deformation using atomistic or mesoscale dislocation dynamics methods. Due to the statistical variability in atomic composition across the slip planes, studies of the motion of long dislocations over sufficiently long trajectories in 3D can enable a meaningful assessment of the kinetic processes involved in glide. With RMPEA uniqueness lying at the atomic scale, molecular dynamics (MD) simulations of mechanically driven dislocation motion have proven ideal for exposing possible mechanisms and trends. Numerous MD studies on RMPEAs have reported unusually wavy and similar glide behavior between screw and edge dislocations and attribute these responses to a rugged landscape in energetic barriers against glide [14,31,32]. MD simulations of screw and edge dislocations in the bcc CoFeNiTi MPEA observed nearly equal mobilities and reduced mobilities relative to those seen in conventional refractory metals [32]. This behavior was reported to be due to the enhanced trapping of segments of dislocation lines in locally unfavorable energetic environments [14]. Among these computational efforts, few have focused on probing the effect of temperature on dislocation glide mechanisms [13,33,34]. MD simulations on the bcc MoNbTaW RMPEA revealed that screw dislocations undergo a distinct cross-kink locking mechanism at elevated temperatures, which could help explain strengthening [13]. Due to length scale constraints inherent to MD techniques, most MD studies treat one or a few samples and short line lengths gliding over short distances [13,31]. They also have time scale limitations and as such impose high stresses or strain rates to shorten the time scales for dislocation motion. Modeling dislocation processes at high temperature calls for capturing thermally activated mechanisms, which would be rare in atomic timescales.

Longer timescales and dislocation lines in MPEAs than MD have been simulated with mesoscale methods, such as discrete dislocation dynamics (DDD), generalized Peierls Nabarro (GPN), kinetic Monte Carlo (kMC) simulations, and phase field (PF) dislocation mechanics simulations [35–38]. Supporting the MD observation, an atomistically informed kMC study showed that cross-kinking mechanisms of screw dislocations can be responsible for the high strength of bcc NbVTa bcc RMPEA [39]. Using kMC combined with DDD, it was demonstrated that thermally activated superjogs can act as pinning points and increase the activation stress of edge dislocations within the strength plateau of the MoNbTaW RMPEA [15]. Integrating the kMC method is an excellent way to achieve diffusive time scales and assess collective behavior but it relies on solid understanding of the important events and their energetic barriers *a priori*. Phase Field Dislocation Dynamics (PFDD) is a 3D, mesoscopic, energy-based modelling approach and like the other mesoscale methods, apart from the kMC studies, has been employed to study dislocations in MPEAs without the effects of temperature [40–43]. Recent versions of the PFDD model for bcc crystals have utilized a bcc computational lattice, which enables reproducing key features of bcc dislocations, such as the nonplanar screw core and the planar edge core, and the anisotropic elastic strain energy outside the core [44]. Consequently, screw/edge character differences in activation stress and mobility, and the ability for the screw dislocations to cross-slip are natural outcomes. For MPEAs, compositional fluctuations in 3D associated with random solid solutions or short-range order are represented by spatial variations in the stacking fault energies [45,46]. Recently, temperature has been successfully incorporated into the PFDD

formulation using a Langevin treatment of the Time Dependent Ginzburg Landau equation [47]. Among the computational methods available, the capabilities of PFDD with Langevin dynamics lie in between MD approaches and kMC-based approaches. Langevin-PFDD simulates dislocation motion due to both atomic-scale composition and thermal fluctuations over longer spatial and temporal scales than MD and with many statistical realizations. Events and their activation barriers are predicted rather than being pre-assigned, and ultimately, any simulated realization identifies the lowest energy pathway and the mechanisms involved.

In this work, we employ Langevin-PFDD to investigate temperature-dependent glide mechanisms in the MoNbTi RMPEA. MoNbTi acts as an exemplar system to evaluate fundamental dislocation mechanisms because it is a single phase, bcc, equiatomic solid solution [5]. Additionally, it is one of the few RMPEAs that exhibits a pronounced strength plateau from approximately 900K-1200K. We aim to quantify and assess screw and edge dislocation mobility in MoNbTi over a range of temperatures where slip is the dominant deformation mechanism, with particular emphasis on the high temperature strength plateau. The role of local chemical fluctuations on dislocation mobility and the glide characteristics at different temperatures and stresses are elucidated and the effects of dislocation glide mechanisms on the experimentally observed strength plateau are discussed. Additionally, line characteristics from initially screw or edge-character dislocations are identified over a range of stress and temperature. We find that a distinct nonplanar kink pair (kp) mechanism of screw dislocations above 900K is likely responsible for the predicted plateau in screw mobility, which in turn may be tied to the strength plateau.

The paper is structured as follows. The next section presents the 3D bcc PFDD model with Langevin dynamics and follows with the construction of statistical realizations of 3D RMPEA crystals with spatially varying energetic landscapes. The results on edge and screw dislocation glide at a range of stresses and elevated temperatures are then presented. We follow with a discussion on the predicted change in glide mechanisms with temperature and their implications on experimental observations of elevated temperature-dependent strength. Finally, we close comparing these findings with prior claims and recommendations.

Phase field dislocation dynamics formulation

PFDD is an energy-based mesoscale model whose full formulation and derivations have been given elsewhere [38]. PFDD tracks the dislocation structure through scalar order parameters $\phi^{\alpha}(\boldsymbol{r})$, which represent the slip on slip system α at a point $\boldsymbol{r}$ in space. Unslipped regions of the crystal of $\phi^{\alpha}(\boldsymbol{r}) = 0$ while slipped regions have $\phi^{\alpha}(\boldsymbol{r}) \geq 1$. Non-integer values of $\phi^{\alpha}(\boldsymbol{r})$ represent the dislocation cores. For a bcc crystal, three slip systems are used, all with Burgers vector $b^{\alpha} = [\bar{1}11]$. The slip plane normals are $n^1 = [110]$, $n^2 = [01\bar{1}]$, and $n^3 = [101]$. $\boldsymbol{\phi}(\boldsymbol{r})$ represents the vector of all $\phi^{\alpha}(\boldsymbol{r})$.

The total energy density ψ of the dislocation system is given by

$$\psi = \psi_{latt}\big(\boldsymbol{\phi}(\boldsymbol{r})\big) + \psi_{elas}\big(\boldsymbol{\phi}(\boldsymbol{r})\big) - \psi_{ext}\big(\boldsymbol{\phi}(\boldsymbol{r})\big) \tag{1}$$

where ψ_{latt} is the lattice energy, ψ_{elas} is the elastic strain energy, and ψ_{ext} is the energy due to an externally applied energy.

The lattice energy for a bcc crystal has the form

$$\psi_{latt}\left(\phi^{\alpha}(\boldsymbol{r})\right) = \sum_{\alpha} \frac{\gamma_{usf}^{\alpha}}{d} \sin^2\left(\pi\phi^{\alpha}(\boldsymbol{r})\right) \tag{2}$$

where γ_{usf}^{α} is the USFE on plane α and d is the interplanar spacing. In an MPEA, γ_{usf}^{α} is dependent on local composition and varies spatially in the simulation cell. The generalized stacking fault energy (GSFE curve) is generated for the {110}<111> system and the USFE is taken as the maximum of the GSFE curves. For refractory pure metals and RMPEAs, both MD and DFT calculations find that GSFE curves can be approximated by a $\sin^2\left(\phi^{\alpha}(\boldsymbol{r})\right)$ function [46,48–52]. Generation of the MPEA crystal with the variable energetic landscape corresponding to a random solid solution will be discussed shortly.

The elastic energy has the form

$$\psi_{elas}\left(\phi^{\alpha}(\boldsymbol{r})\right) = \frac{1}{2} C_{ijkl} \epsilon_{ij}^{e}\left(\boldsymbol{\phi}(\boldsymbol{r})\right) \epsilon_{kl}^{e}\left(\boldsymbol{\phi}(\boldsymbol{r})\right) \tag{3}$$

where C_{ijkl} is the elastic stiff tensor and ϵ_{ij}^{e} is the elastic strain.

The external energy has the form

$$\psi_{ext}\left(\boldsymbol{\phi}(\boldsymbol{r})\right) = \sigma_{ij}^{app} \epsilon_{ij}^{p}\left(\boldsymbol{\phi}(\boldsymbol{r})\right) \tag{4}$$

where σ_{ij}^{app} is the applied stress state and ϵ_{ij}^{p} is the plastic strain.

For the time evolution of the order parameters, we use the stochastic Time-Dependent Ginzburg-Landau (TDGL) equation, also known as the Langevin Equation [53,54]:

$$\frac{\partial \varphi^{\alpha}(\mathbf{r},t)}{\partial t} = -M \frac{\delta \psi}{\delta \varphi^{\alpha}(\mathbf{r},t)} + \theta(\mathbf{r},t) \tag{5}$$

where M is the relaxation coefficient. The statistically fluctuating term $\theta(\mathbf{r},t)$ is conventionally represented by a Gaussian distribution with zero first moment and second moment equal to $2k_B TM\delta(t-t')\delta(\mathbf{r}-\mathbf{r}')$ where k_B is Boltzmann's constant and T is absolute temperature [55]. The distribution is representative of fluctuations that are uncorrelated in both space and time and uncorrelated between discrete steps. The simulation description of the fluctuations is obtained by successively sampling a random number $\theta(n,m)$ [55]

$$\theta(n,m) = \sqrt{\frac{2k_B TM}{\Omega\, t}} \rho_i \tag{6}$$

where Ω is volume and $\rho\{\rho\colon \rho_i\ ,\ i=1,\dots\}$ is an i.i.d. random number from a Gaussian N(0,1) distribution.

The following discrete form of the TDGL between the time increments t and $t+\Delta t$ is

$$\varphi^{\alpha}(\mathbf{r},t+\Delta t) = \varphi^{\alpha}(\mathbf{r},t) - M\Delta t\frac{\partial\psi}{\partial\varphi^{\alpha}(\mathbf{r},t)} + \int_{t}^{t+\Delta t}\theta(\mathbf{r},s)ds \tag{7}$$

The dimensionless equation is expressed as

$$\varphi^{\alpha}(\mathbf{r},\tau+\Delta\tau) = \varphi^{\alpha}(\mathbf{r},\tau) - \Delta\tau\frac{\partial\psi^{*}}{\partial\varphi^{\alpha}(\mathbf{r},\tau)} + \int_{\tau}^{\tau+\Delta\tau}\theta^{*}(\mathbf{r},s)ds \tag{8}$$

which is used in performing the computations. The normalized time increment $\Delta\tau$ and free energy ψ^{*} are

$$\Delta\tau = M\mu\Delta t \tag{9}$$

$$\psi^{*} = \frac{\psi}{\mu} \tag{10}$$

where μ is the shear modulus, and the dimensionless Langevin fluctuation $\theta^{*} = \theta/M\mu$ is

$$\theta^{*}(n,m) = \sqrt{\frac{2k_BT}{\eta\,\Delta\tau}}\rho_i \tag{11}$$

where $\eta = \Omega\mu$.

Material and model set up

The elastic stiffness tensor, ***C***, and lattice parameter, *a* are inputs to the PFDD formulation. In the current study, we assume that these parameters do not change spatially or with temperature. Their average quantities for MoNbTi were calculated using DFT (see Supplemental Material for more details on DFT methodology [56] which includes Refs. [57–66]). The elastic constants are C_{11} = 252.13 GPa, C_{12} = 134.11 GPa, and C_{44} = 32.41 GPa and lattice constant a = 0.3225 nm [57]. The elastic constants of this RMPEA have been shown to have a weak dependence on deviations in composition [46]. While the temperature dependence of their elastic constants is unknown, we note that some RMPEAs display a weak temperature dependence [67]. The slight continual reduction in elastic constants, however, is insufficient to explain the strength plateau of RMPEAs.

The time increment, $\Delta\tau$, must be chosen fine enough to capture the formation of a kp but coarse enough to allow for a sufficiently large number of fluctuations to occur within it and to be adequately represented by a Gaussian distribution. The Debye frequency ϖ of the refractory metals

included in this MPEA are all on the order of 10^{13} Hz [68], (e.g., ϖ = 10^{13} Hz for Mo, 3.5 x 10^{13} Hz for Ti, and 3 x 10^{13} Hz for Nb). In all PFDD simulations that follow we choose Δt as $\Delta t = 1000/\varpi = 4x10^{-11}s$, which permits for a very large number of thermal fluctuations per Ω.

In each PFDD simulation, the 3D simulation grid is defined by the primitive vectors $p^1 = \frac{b}{\sqrt{3}}[11\bar{1}]$, $p^2 = \frac{b}{\sqrt{3}}[\bar{1}11]$, and $p^3 = \frac{b}{\sqrt{3}}[1\bar{1}1]$. Screw and edge simulations employ periodic boundary conditions in all three directions. For screw dislocation simulations, a 128 x 128 x 128 simulation cell is used, while for edge simulations, a 128 x 384 x 128 simulation cell is used. The simulation grid is set up such that the grid points align with atomic sites in a bcc lattice and the grid spacing λ is equal to one Burgers vector, *b*. It was previously shown that there was no detectable length dependence on the critical glide stress of edge or screw dislocations in MoNbTi longer than 25 nm [69]. As such, both dislocation types in the current study were > 25 nm. The initial dislocation dipole is placed on the (110) slip plane by setting $\phi^1 = 1$ between the two dislocations. An example of a non-orthogonal bcc screw dislocation dipole setup for a PFDD simulation is shown in Fig. 1. Five realizations were performed at each temperature and stress level.

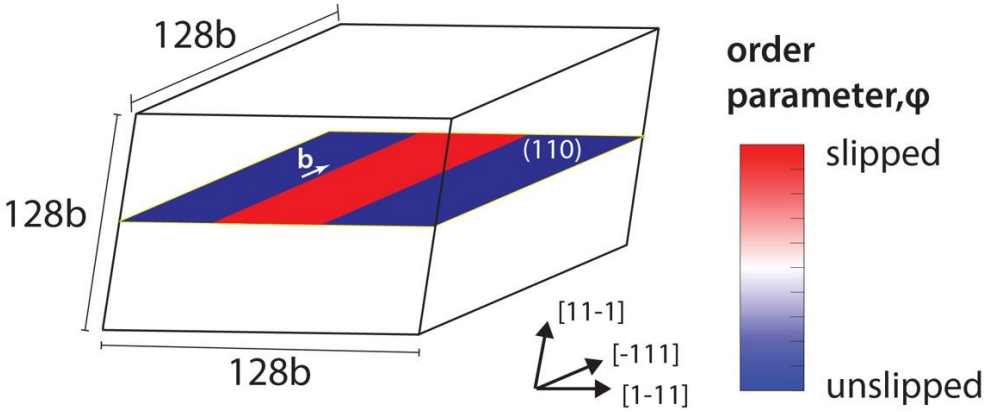

FIG. 1. *Setup for a screw dislocation dipole placed on the (110) plane in a non-orthogonal bcc computation grid.*

The applied stress state σ^{app} is a simple shear given by

$$\sigma^{app} = \begin{pmatrix} 0 & 0 & 0 \\ 0 & 0 & \sigma \\ 0 & \sigma & 0 \end{pmatrix}$$

The σ^{app} tensor is rotated such that the 2-direction align with the Burgers vector and the 3-direction aligns with the normal of the maximum resolved shear stress (MRSS) plane. The values σ used in simulation were chosen to encompass the experimental yield strengths of MoNbTi over a broad temperature range. These ranged from as high as $\sigma^{exp} = 0.034\mu$ at 300K to as low as $\sigma^{exp} = 0.01\mu$ at 1500K, where μ is an effective isotropic shear modulus 32.3 GPa. To cover these, we considered three levels: $\sigma = 0.01\mu$ (low), $\sigma = 0.02\mu$ (medium), and $\sigma = 0.03\mu$ (high). The melting temperature of MoNbTi is T_{melt} ~ 2400K [20]. With the transition of dislocation-mediated plasticity to diffusion-mediated plasticity typically occurring at ~ $0.5T_{melt}$, test temperatures in simulation ranged from 600K to 1300K.

To create the variable USFE values for MoNbTi, a regular bcc atomic lattice with a uniform distribution of elements with no chemical short-range order (CSRO) is generated [70]. The local atomic composition at each order parameter for each grid point is defined by the atoms within a 2*b* radius within the slip plane of the order parameter. The local atomic compositions are then converted to local USFE values using USFE composition maps that were calculated previously with molecular statics [71]. The local USFE values are used during PFDD simulations. Since screw-oriented dislocations can cross slip and hence glide pathways can be 3D, this procedure is applied for all three {110}-type slip planes (order parameters) in the cell. Figure 2 shows an example of the variable USFE random solid solution MoNbTi for a screw dislocation. We note that although this methodology can produce structures that exhibit CSRO [70], atom probe tomography of MoNbTi single crystals did not shown evidence of CSRO [5].

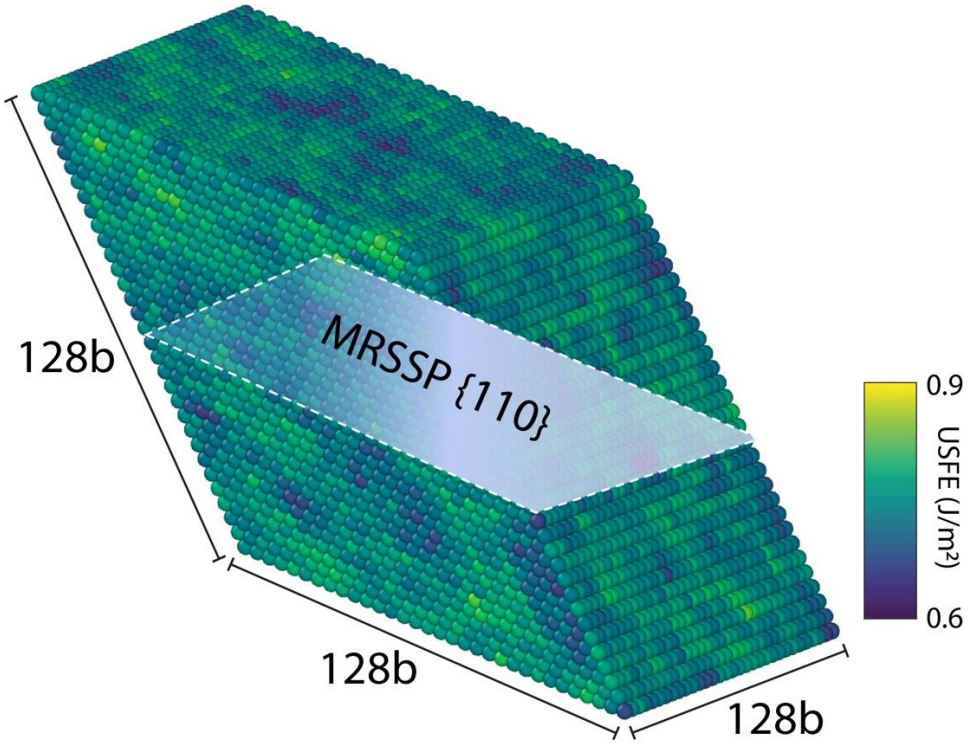

FIG. 2. *One sample of the variable energetic computational cell of random solid solution MoNbTi used in PFDD simulations. The dislocation dipole is not included in the schematic. The central {110} plane is the maximum resolved shear stress plane (MRSSP).*

Results

Edge Dislocation Motion

Prior to examining the effect of a driving stress on the edge dislocation, we first observe the characteristics of a relaxed edge dislocation under zero stress at elevated temperatures of 600K, 1200K, and 1300K over a long period of time of a few thousand timesteps. At 600K, 1*b* wide segments of the dislocation line randomly jump 1*b* forwards and backwards from the initial line position on the habit plane. This "random fluttering" can give the dislocation an overall wavy appearance with an average wavelength of ~40*b*. At 1200K, the frequency of the fluttering increases and the average amplitude of the now wavy dislocation increases to several *b*, and

average wavelength decreases to ~20*b*. By end of the simulation, the average line position has not advanced. Significantly, at 1300K the amount of thermal kink pairs (thermal kps) in the system, which range from 1*b*-3*b* in width, is sufficient to move the dislocation forward by 2*b*.

Figure 3 presents edge propagation distance, d as a function of time, τ for one of the five realizations tested. When a low stress is applied to an initially straight dislocation line (Fig. 3(a)), there is an initial delay time τ_0 (i.e., the time required for first propagation event) at the lowest testing temperature of 700K. Due to thermal activation, kink pairs (kps) of various widths form at random positions along the dislocation line. In time, their location and widths change, but the nominal location of the dislocation line does not advance until $\tau_0 = 600$. Once glide begins, the dislocation experiences two waiting periods τ^*, where the dislocation line is pinned for $\tau^* = 100$ before glide continues. As temperature increases from 700K to 1200K, the waiting periods decrease, and by 1000K, $\tau^* = 0$ and glide becomes smooth. Here glide is deemed to be nominally smooth in time when the waiting periods τ^* are much less than gliding periods τ_{glide}.

Dislocation glide behavior under the medium and high stress levels are examined in Figs. 3(b) and 3(c), respectively. Under medium stress, the longest delay time of $\tau_0 = 400$ occurs at the lowest temperature (600K). Under high stress, the longest delay time of $\tau_0 = 200$ again occurs at the lowest temperature, but half of the time to initiate glide under medium stress at the same temperature. Unlike the low stress condition (Fig. 3(a)), no waiting periods are observed at any temperature tested under these two stress levels. Glide is smooth once the edge dislocation begins moving. Results of the propagation distance are replotted versus temperature two different times $\tau = 500$ and $\tau = 1000$ (Fig. 3(d)). Comparing the two times at the lowest stress shows that the edge dislocation requires some amount of time ($\tau > 500$) to move more than 5*b* for all temperatures. The $\tau = 1000$ indicates that the edge dislocation moves smoothly with the exception of the lowest stress and temperatures at or below 600K. The sensitivity to temperature on propagation distance becomes apparent.

To gain insight on how an edge dislocation accomplishes smooth glide through the rugged energetic landscape of MoNbTi, the line morphology is studied at different temperatures and stresses. In Fig. 4, the morphologies of the dislocation lines at various points in time for a few sample temperatures are examined for the low (Fig. 4(a)), medium (Fig. 4(b)) and high (Fig. 4(c)) stress levels at $\tau = 1000$, with insets at intermediate moments $\tau = 200$ and $\tau = 500$. Under the low stress condition at 1200K (Fig. 4(a)), numerous kps form in the direction of shear on the habit plane and they accumulate along the line, giving the line a significantly wavy appearance. This signifies that kp nucleation is much easier than sideways kp migration. This accumulation of kps is conventionally referred to as overlapping kp motion [72]. The basic dominance of kp nucleation over migration is an expected consequence of the greater Peierls stress for a screw element than an edge element. Forming a kp on an edge dislocation line creates two screw side segments that are relatively difficult to migrate. While the screw-to-edge ratio in Peierls stress in MoNbTi is less than 5, at least two orders of magnitude lower than a pure bcc metal, kp formation is still overpowering [5,73]. The edge dislocation propagates forward via overlapping kp motion over the entire simulation time. Similar glide behavior is observed under medium stresses at 900K, as shown in Fig. 4(b). Glide is also mediated by the formation of overlapping kps in random amounts along the length and a stochastic, wavy morphology manifests. Fig. 4(c) shows that under even higher stresses but at 600K, the same overlapping kp glide mechanism and wavy line morphologies

are also observed. The glide behavior seen in these few examples represent that seen in all realizations and at all temperatures and stress levels for edge dislocations.

It is an interesting observation that the basic overlapping kp mechanism enabling edge dislocation glide in MoNbTi at elevated temperatures ($T \geq 600K$) is unaffected by stress and temperature. Further, the average amplitudes and wavelengths of the gliding wavy lines are not influenced by stress or temperature. More remarkably, we find no indication that the highly protruded portions of the line correspond to areas of relatively low USFE. Based on prior studies, relatively high USFE regions randomly encountered by the moving dislocation are thought to act as local pinning points [74]. However, these previously reported observations are usually made at 0K or much lower temperatures than considered here. In our simulations, increasing temperature across the elevated temperature regime for this material serves to increase the frequency of kp nucleation and the rate at which the dislocation line glides.

The edge character of these dislocations only refers to their initial state. As evidenced by the insets in Fig. 4, as kps form along the line, many screw-character segments form. As kps accumulate (or overlap), the overall character of the initial edge dislocation-oriented line becomes mixed during glide. Thus, many elementary glide processes common to edge dislocations, like climb or jog formation, would become limited in RMPEAs.

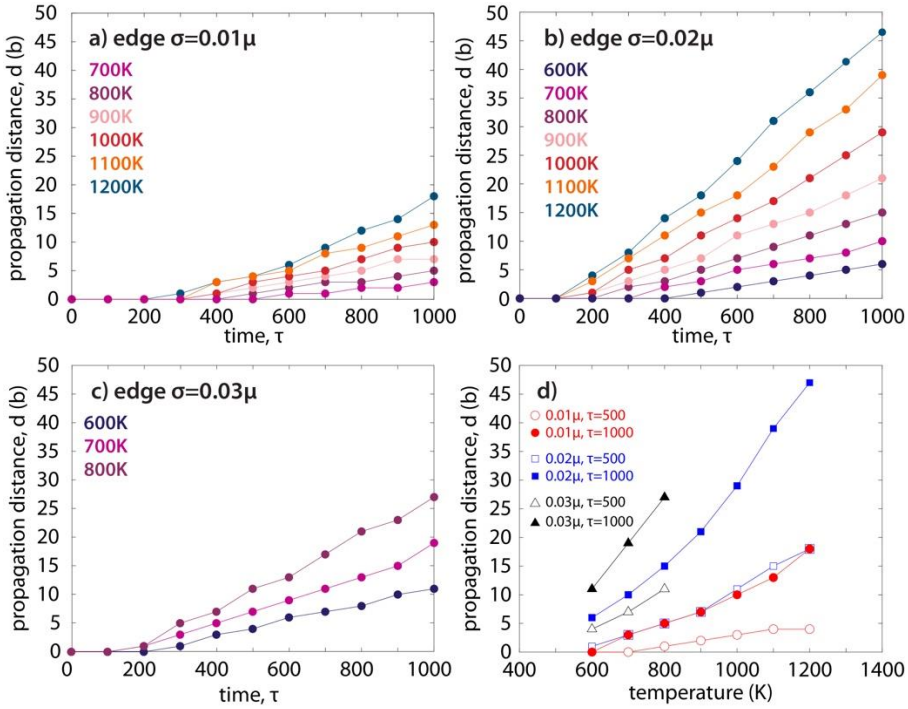

FIG 3. *Propagation distance as a function of time for a long initially edge-character dislocation on the (110) habit plane in MoNbTi under an applied stress of (a) $\sigma = 0.01\mu$, (b) $\sigma = 0.02\mu$, and (c) $\sigma = 0.03\mu$. (d) Propagation distance plotted versus temperature for $\sigma = 0.01\mu$, $\sigma = 0.02\mu$, and $\sigma = 0.03\mu$ at two different times, $\tau = 500$ and $\tau = 1000$.*

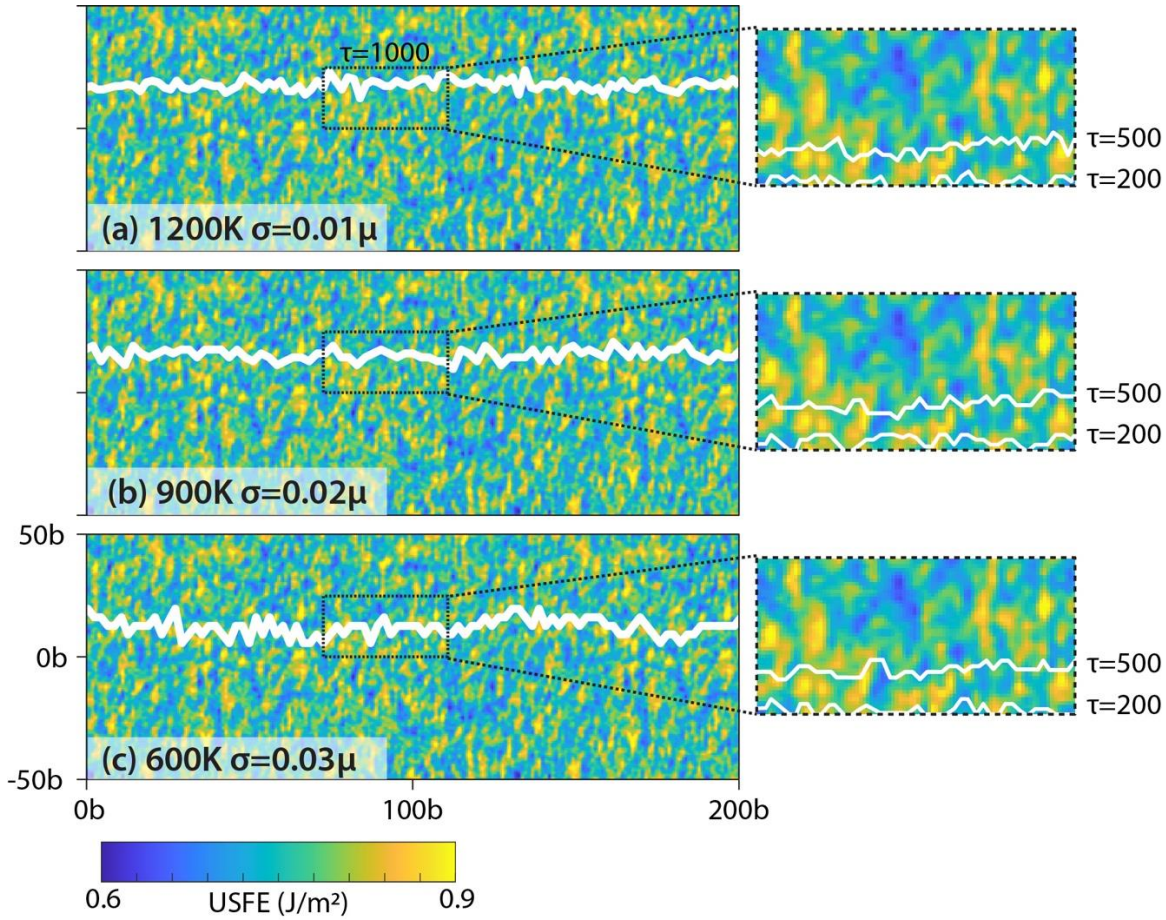

FIG. 4. *Snapshots of the initially edge-character dislocation line at τ = 1000 at and insets of line position at τ = 200 and τ = 500. (a) 1200K, $\sigma = 0.01\mu$ (b) 900K, $= 0.02\mu$ and (c) 600K, $\sigma = 0.03\mu$. The colored surface indicates values of the USFE.*

PFDD simulations of glide of starting edge dislocations in MoNbTi have been previously performed at 0K [46]. In 0K simulations, edge glide is jerky and can eventually stop after some amount of glide. Every time it arrests, the applied stress needs to be raised to restart motion. In contrast, as shown here, at finite and elevated temperatures, once an edge dislocation starts to glide, it will continue in a smooth manner and no additional stress is necessary. Also seen in the 0K simulations, the line morphology of the moving dislocation is wavy, with many non-edge segments protruding forward between sites held back at exceptionally high USFE regions along the line. Thus, at 0K, the waviness stems solely from the local fluctuations in USFE. At elevated temperatures, however, thermal fluctuations also contribute to the wavy morphology and as mentioned already, the correlation with USFE obscured.

Screw Dislocation Motion

Prior to examining the effect of a driving stress on the screw dislocation, we first investigate the characteristics of a relaxed screw dislocation under zero stress at elevated temperatures 600K, 1200K, and 1300K. At 600K, 1*b* segments of the dislocation line undergo random fluttering forwards and backwards, usually 1*b*, from the initial line position. By the end of the simulation time, the dislocation line has not advanced and still generally maintains a straight configuration.

At 1200K, wider segments (>1*b*) of the dislocation line, or kps, jump forwards or backwards at random times and sites along the line. At any given time, a kp is identified as region where at least three contiguous sites along the dislocation line have advanced normal to it. Two adjacent kps must be separated by at least one atomic site to be distinct. The entire dislocation has moved one Burgers vector when at least 90% of the sites along the line have advanced at least one Burgers vector. Unlike at lower temperatures, the fluttering kps can extend several *b* in height. These kps can form on the habit plane as well as any of the two cross-slip planes. Some of these nonplanar kps recede to the habit plane, while others remain on the cross-slip plane for the entire simulation time. By the end of simulation, the average position of the dislocation has not advanced, but is wavy due to nonplanar and planar kps that have persisted throughout simulation. Finally, at 1300K, the dislocation line exhibits similar dynamics to the 1200K case, but this time, these thermal kps persist throughout the simulation and migrate, advancing the dislocation line by 2*b*. Thus, under zero stress, the screw dislocation state at finite temperature may have pre-existing narrow kps. Other reports using MD have noted similar pre-kinked screw dislocations in RMPEAs under zero stress, claiming that this means kp activation is easy in RMPEAs compared to refractory constituents [14]. Here we show that these initial kps require thermal fluctuations and hence their exact configuration stochastic and frequency temperature dependent.

Figure 5 shows a representative propagation distance d vs. τ curves from one among five realizations for each temperature and each stress for a finite amount of time. Under the lowest stress and lowest temperature (600K), within this period, the dislocation line in this case advances 1*b* after a long delay time of $\tau_0 = 1800$. During this initial delay period, random sites along the dislocation line fluctuate 1*b* forward in the glide plane and then recede back to their original location. At both 600K and 700K, the dislocation only moves 1*b* over the simulated period. As temperature increases to 800K, the delay period τ_0 decreases, and the position of the line moves forward 2*b* and remains in wait for the rest of the simulation time. From 900K to 1200K, the τ_0 decreases further and over the remaining simulation time, glide is characterized by an alternating stop/start motion. The waiting periods τ^* between moments of glide range from $\tau^* = 100$ to $\tau^* = 300$ (Fig. 5(a)). The average delay time and wait times decrease, leading to a concomitant increase in the maximum distance propagated. As before for edge dislocations, we define smooth glide as when the waiting periods are equal to or less than gliding periods. By this definition, we can detect a jerky to smooth glide transition when $T \geq 1000$K.

Under medium stress (Fig. 5(b)), as seen under low stress, screw motion displays similarly long delays τ_0 before glide initiates and jerky behavior in time after it initiates. Compared to the lower stress, for the same temperature, the delay times τ_0 are shorter and many more waiting periods τ^* are detected between spurts of glide. Similar temperature sensitivities are seen, such as τ_0 and τ^* decreasing and the maximum distance propagated increasing with temperature. A transition from jerky to smooth glide occurs at a lower temperature of 900K. The interesting difference is that the dislocation propagates the same amount 10*b* from 1100K–1200K. While this specific result may be a coincidence, arising from random sampling and the fixed simulation time, it is a sign of a possible temperature insensitivity, a point we return to shortly.

Under high applied stress (Fig. 5(c)), similar temperature-dependent glide behavior is seen. At the lowest temperature 600K, the dislocation moves 2*b* after $\tau_0 = 300$. As temperature increases to 1000K, τ_0 decreases further. For $T > 1000$K, any time delay τ_0 or stop/start glide behavior becomes

undetectable. The propagation vs. time curves become like those observed for edge dislocations. By the same definition for smooth glide as before, glide becomes smooth at a relatively low temperature of 700K.

Results of propagation distance at the three stress conditions are replotted versus temperature and shown in Fig. 5(d) at $\tau = 500$ and $\tau = 1000$. At lower stress and $\tau = 500$, the dislocation does not advance by more than $2b$ until $T > 1000$K. At $\tau = 1000$, only the high stress condition displays a strong sensitivity to temperature, whereas the other two stresses display temperature insensitive propagation over certain regions.

To analyze glide mechanisms, the morphologies of the entire line are examined over time. Figs. 6(a)-(c) display typical samples among the several realizations for some extreme cases, with the position of the screw dislocation at the end of the simulation overlaid on the map of the unstable stacking fault energy (USFE) assigned to the glide plane. The insets show close ups during both wait and glide periods. Recall that under no stress but finite temperatures, thermal energy alone causes the dislocation to fluctuate both forward and backwards with noncritical kps forming in all allowable directions and then receding. At low stress but high temperature 1200K (Fig. 6(a)), there is sufficient stress to nucleate and migrate kps along the dislocation line that propagate the screw forward. In some parts of the line, the kps accumulate and overlap. As such, the dislocation adopts a wavy morphology with many edge side-segments present along the line. The inset of Fig. 6(a) shows the line morphology during a wait period (white) and a glide period (red). Interestingly, both snapshots show the presence of overlapping kps leading to random amplitudes along the dislocation line, with little noticeable difference between the two states. Additionally, there is no evidence that kps propagate further in regions of low USFE, or that nucleation/migration is inhibited by regions of high USFE. This underscores the statistical nature of glide at high temperature, where the difference between a glide period and a wait period only depends on the number of energetically favorable sites at which the dislocation line can form and migrate a kp. Temperature is seen to affect the amplitude of the wavy line. In the case of medium stress and a relatively lower temperature of 900K, in Fig. 6(b), the dislocation again glides via overlapping kp formation, but the amplitude is less than seen in Fig. 6(a).

In contrast to Figs. 6(a) and 6(b), in Fig. 6(c) at 600K and high stress, the screw glides via the nucleation and expansion of multiple, closely spaced kps that form along the dislocation line. The kps do not overlap and each kp is distinct. The inset shows that multiple kps are present both while in the waiting periods (white) and glide periods (red). A critical width to nucleate a stable kp that will proceed to migrate can be identified and is on average approximately $3b$. Narrower kps tend to recede. These kps form at locations of relatively low USFE and thus the motion exhibits a correlation with the underlying composition fluctuations not seen before at higher temperatures. This discrete kp glide behavior is more closely aligned with the distinct kp formation and migration behavior expected of screw dislocations in refractory alloys and the anticipated influential role of the rugged energetic landscape, characteristic of RMPEAs. But we emphasize that this so-called expected behavior emerges only in a specific stress/temperature regime.

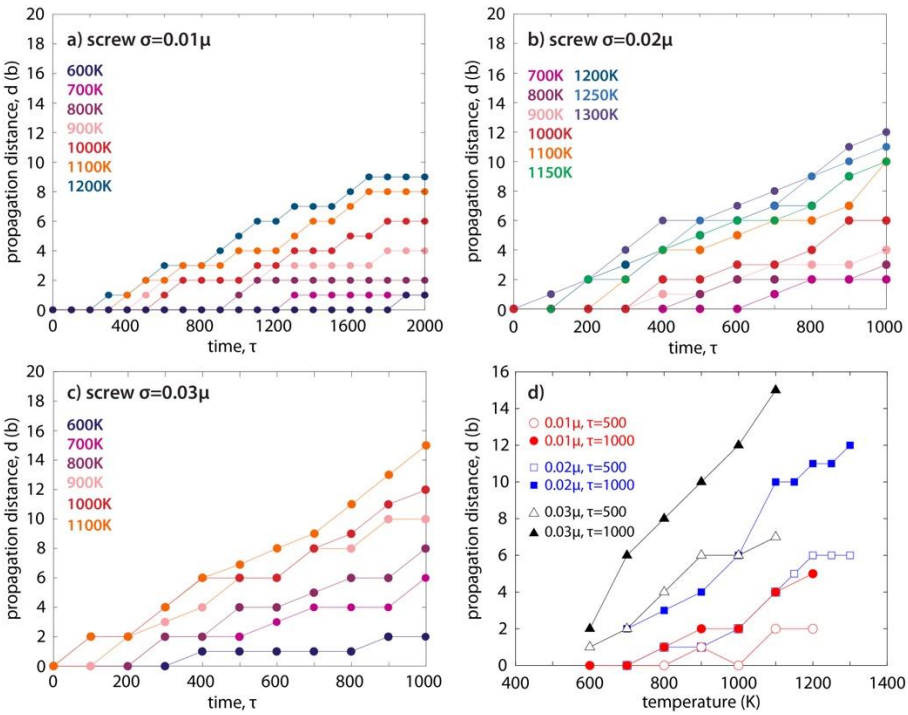

FIG 5. *Propagation distance as a function of time for a long initially screw-character dislocation on the (110) habit plane in MoNbTi under an applied stress of (a)* $\sigma = 0.01\mu$*, (b)* $\sigma = 0.02\mu$*, and (c)* $\sigma = 0.03\mu$*. (d) Propagation distance plotted versus temperature for* $\sigma = 0.01\mu$*,* $\sigma = 0.02\mu$*, and* $\sigma = 0.03\mu$ *at two different times,* $\tau = 500$ *and* $\tau = 1000$*.*

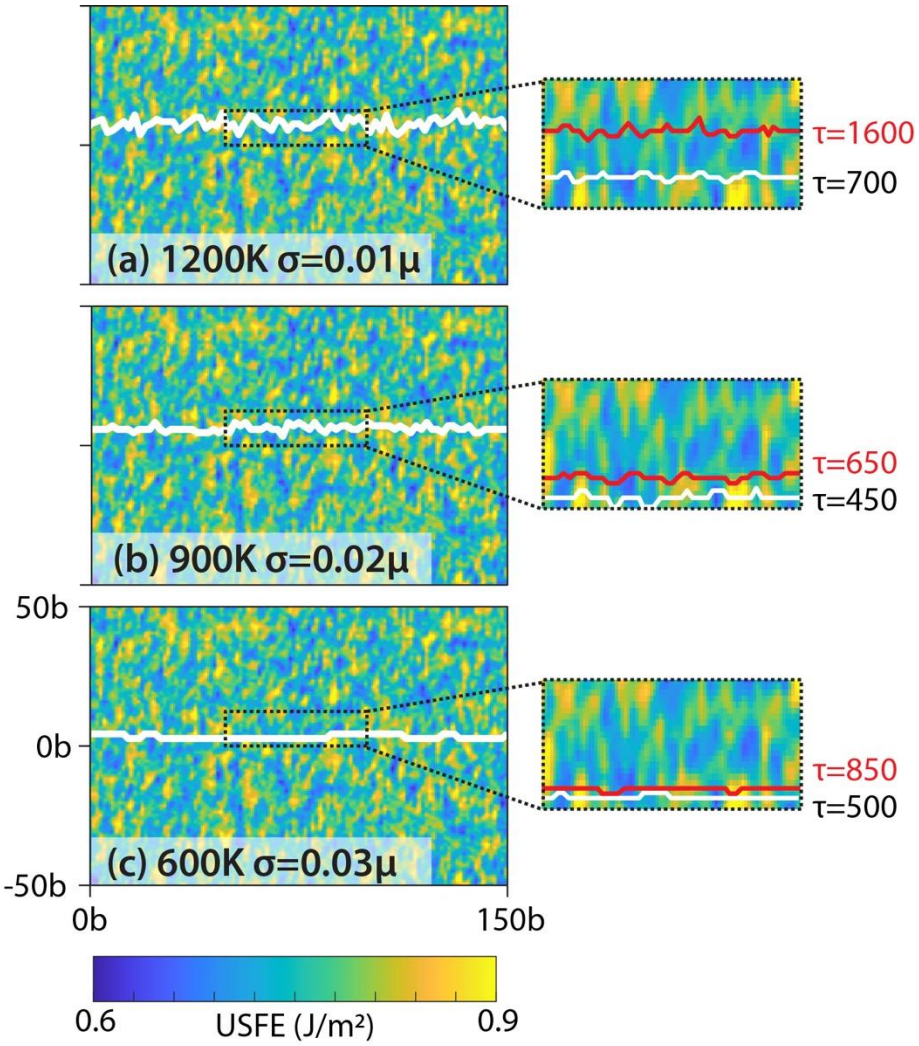

FIG. 6. *Snapshots of a screw dislocation line at end of simulation time τ at temperatures of* ***a)*** *1200K* ***b)*** *900K, and* ***c)*** *600K. Insets at two previous timesteps are shown for each condition. A snapshot of the dislocation in motion is shown in red and an instance of the dislocation in a dwell period is shown in white. The colorbar indicates values of the USFE on the surface plots. Snapshot in (a) is taken under low stress $\sigma = 0.01\mu$ and at τ=2000, (b) medium stress $\sigma = 0.02\mu$ and at τ=1000, and (c) high stress $\sigma = 0.03\mu$ and at τ=1000.*

As screw dislocations glide through the rugged landscape, cross slip is possible even if the applied shear is only resolved on the habit plane. To identify cross-slip events, we analyze the 3D pathway along the dislocation and over a large trajectory of the glide plane. As an example, Fig. 7 shows one of the five realizations of the dislocation path under the medium stress level after so many time steps at different temperatures. At 800K and above, a fraction of the kps is seen to form on one of the two cross-slip planes at various positions along the line rather than the habit plane. These cross-slipped kps do not migrate nor do they continue to glide on the cross-slip planes. We refer to them as *nonplanar kps*. As the portions of the dislocation on the habit plane adjacent to these nonplanar kps continue to glide on the habit plane, the nonplanar segments of the dislocation are left behind on the cross-slip plane and remain immobile for the rest of the simulation time (appearing as orange in Fig. 7).

To determine any influence of temperature and stress, Figure 7(e) plots the total number of nonplanar kps accumulated at the end of the simulation as a function of temperature for all three stresses. Nonplanar kps are detected at 700K and the amount is similar for all three stress levels. For T > 900K, this fraction becomes stress dependent and higher amounts of nonplanar kps form under lower stress levels. This implies that nonplanar kps result from proportionally greater contribution of thermal energy, which are 3D and nearly isotropic, than mechanical energy, which are 2D and anisotropic. The large amplitudes of the wavy dislocation line seen in Fig. 6(a) from 900K to 1200K are partly the result of the increased amount of nonplanar kink debris formed in the wake of the dislocation. Although the screw glides via the formation of overlapping kps, nonplanar kps cause a heightened waviness because the dislocation must continue to glide on the habit plane around the nonplanar kp debris. Interestingly, we find no evidence that the formation of nonplanar kps is related to jerky glide. Glide is jerky whether nonplanar kps form or not.

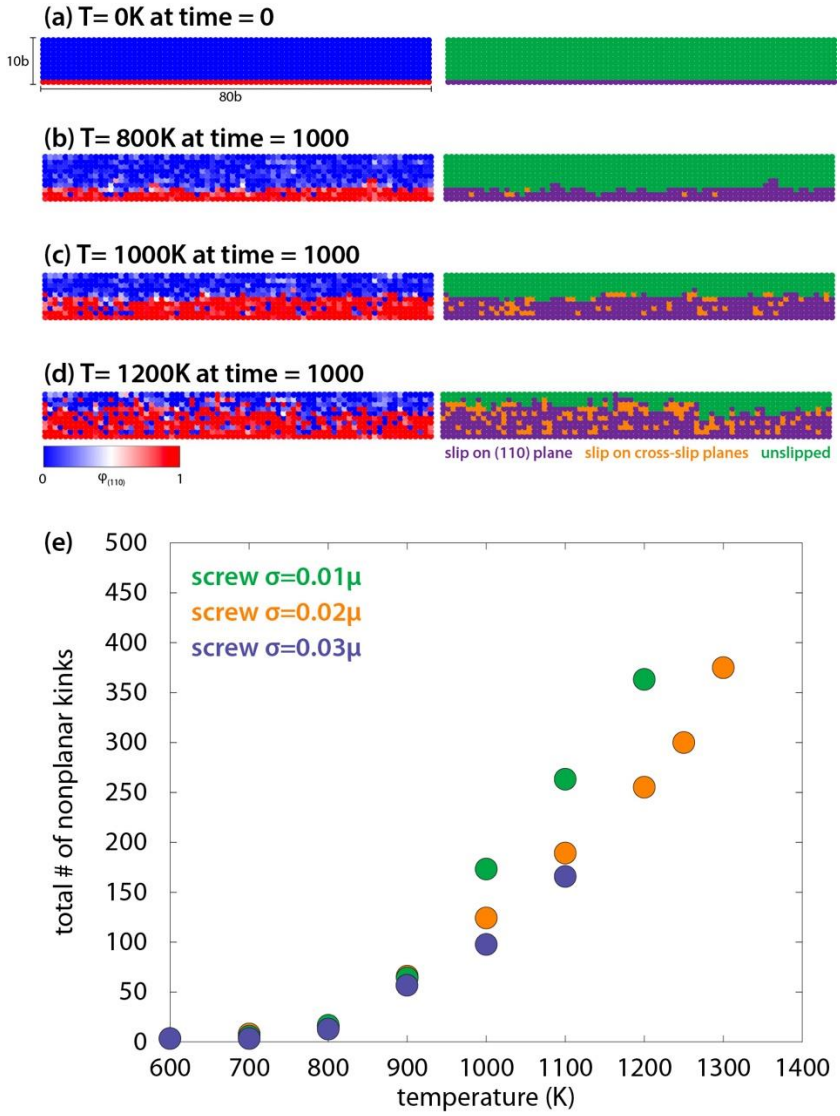

FIG. 7. *Slipped regions of MoNbTi by a screw dislocation initially placed on the (110) habit plane under medium driving stress. (a) the initially straight screw dislocation at 0K and $\tau = 0$. For the left column, the boundary between $\varphi_{(110)} = 1$ (red) and $\varphi_{(110)} = 0$ (blue) is the initial position of the dislocation. For the right column, the snapshots*

track: 1) the unslipped regions (green) where the order parameter on the habit plane and two cross slip planes are zero, 2) the slipped (110) plane (purple) where order parameter $\varphi_{(110)} > 0.8$ and order parameters of the two cross slip planes are zero (i.e., $\varphi_{(101)} = \varphi_{(01-1)} = 0$, and 3) regions of the crystal that undergo slip via nonplanar kps (orange) corresponding to the condition that $\varphi_{(101)}$ and $\varphi_{(01-1)} > 0.8$ and $\varphi_{(110)} = 0$. (b, (c), and (d) shown at end of simulation. (e) Number of nonplanar kps as a function of temperature for low, medium, and high stress levels.

Figure 8 shows the effective mobility for the entire screw dislocation line for the stress/temperature conditions in which glide velocity was smooth (not jerky) under constant applied stress. As shown, this regime manifests at high temperatures, starting at 700K for the highest stress level. Dislocation mobility is determined by $m = \frac{v}{b\sigma}$, where v is the effective screw velocity over sufficiently long time of glide. We observe that m displays negligible stress dependence but three regimes in temperature. From 700K, m rises with temperature, then plateaus from 1100K–1200K, and finally when temperatures exceed 1200K, m increases rapidly. The regime of "sluggish mobility" in temperature from 1100K–1200K would suggest a window of temperature-insensitive strength, i.e., the strength plateau. This sluggishness is distinct from the often reported sluggish mobility of screw dislocations in RMPEAs, which usually refer to slower moving screw dislocations in RMPEAs relative to their constituents at fixed temperature.

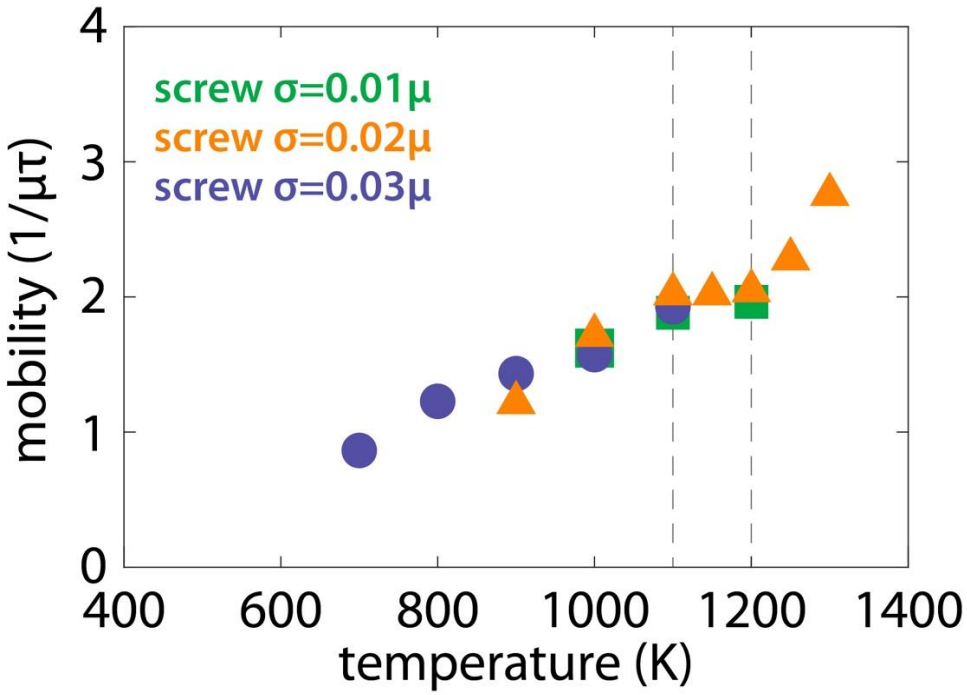

FIG. 8. *Screw mobility for three applied stresses plotted versus temperature. Mobility is taken as dislocation velocity normalized by applied stress and Burgers vector magnitude. Mobility is only plotted for temperature conditions at which a steady state velocity could be computed (i.e., waiting time<travel time). Screw dislocations display a temperature insensitive mobility from T=1100K-1200K.*

Fig. 9 summarizes the various screw dislocation glide mechanisms observed here at elevated temperatures. At the relatively low stresses or temperatures, the screw glides via the nucleation and growth of multiple kps along the dislocation line (Fig. 9(a)). This regime is marked by long wait times, jerky glide, and a small dislocation line amplitude. In the moderate stress/temperature regime, overlapping kp motion is observed (Fig. 9(b)). Overlapping kps along the dislocation line

result from nucleation rates exceeding sideways migration rates. Dislocation line amplitudes are larger and wait times are lower than the multiple kp regime. At T≥900K, screws glide via overlapping kp motion and nonplanar kp formation, the latter leaving a large population of debris in the wake of the slipped region (Fig. 9(c)). Figure 9(d) presents these glide mechanisms on an elevated temperature-stress map. Quantitatively, the temperature-stress regimes on this map are specific to MoNbTi, but changing to another solid solution RMPEA should not affect the general description of these regimes for screw dislocations.

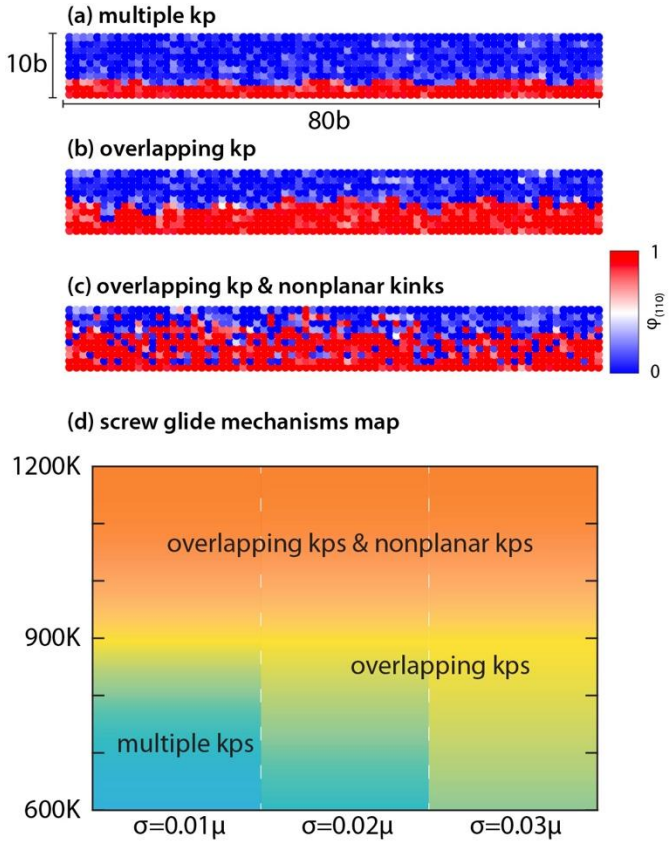

FIG. 9. *Summary of screw glide mechanism regimes (a) multiple kp, (b) overlapping kp, and (c) overlapping kp and nonplanar kp regimes. (d) screw glide mechanisms map across temperature and stress conditions. Quantitatively, the temperatures and stresses corresponding to the boundaries between regimes apply to MoNbTi, but the regimes are expected for screw dislocations in other RMPEAs.*

Previously the motion of long screw dislocations was studied in MoNbTi using PFDD at 0K [46]. In the absence of thermal fluctuations, the screw dislocation moved by forming kps in locally low USFE regions. Under a constant shear stress, the dislocation could only move so far before gliding into a region where no kp could form along its length since the driving stress was not sufficient to overcome the local USFE anywhere. The applied stress had to be incremented to form a new kp and restart motion. The dislocation was wavy in glide but nearly straight when arrested. This stop/start behavior made glide characteristically jerky. In the present simulations, at finite temperatures and under much lower stresses, however, we find the dislocation can glide under constant stress provided it is given time to wait for a sufficiently large thermal jump to locally overcome the relatively harder regions in the rugged energetic landscape for kp formation or migration. As the screw glides, its morphology is always wavy, even when it is arrested and

waiting between advances. Glide proceeds in a jerky manner due to the stop/start behavior between successively random waiting times.

Discussion

As mentioned, one of the most salient features of some RMPEAs is their ability to retain high strength at elevated temperature and the underlying mechanisms have yet to be clarified. Figure 10 plots the experimental yield stress together with the PFDD screw mobility versus temperature. The high, medium, and low stress conditions at which mobility is calculated are indicated on the experimental curve with dashed grey lines. The comparison indicates an overlap between the yield strength plateau (900K–1280K) and screw mobility plateau (1100K–1200K). In the calculations, the latter is related to a rise in the frequency of nonplanar kps, which becomes significant at 900K (Fig. 7(e)), the same temperature at which yield strength temperature insensitivity begins. The results suggest that temperature-induced sluggish screw mobility from the increased number of nonplanar kps contributes to the strength plateau in MoNbTi. They also implicitly indicate that the glide of screw dislocations may be the rate controlling mechanism in the high temperature deformation of the MoNbTi system.

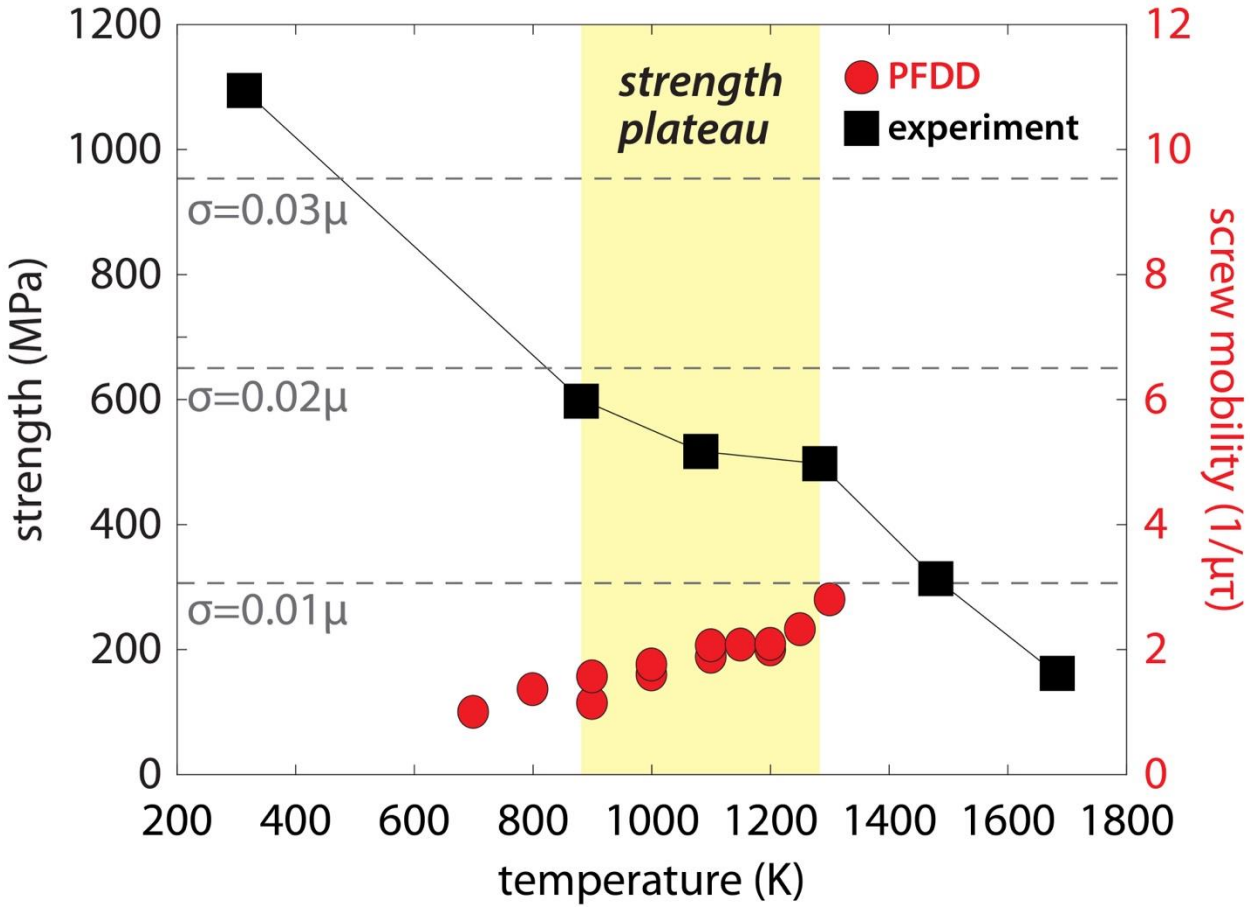

FIG. 10. *Comparison of temperature insensitive strengths from experimental data on MoNbTi and PFDD results on screw mobility.*

The macroscopic yield and screw mobility also both change after the plateau, above T > 1200K, in a way that would suggest screw dislocation motion continues to play a dominant role even at high temperatures. Specifically, the screw dislocation mobility begins to increase, and the material yield stress to soften T > 1200K. From the calculations, however, there is no marked change in the rate of kp and nonplanar kp formation. Both events uniformly increase starting from 800K. There is no dissolution or removal of nonplanar kps at 1200K and beyond. Further, screw glide is smooth (non-jerky) for all stress levels starting from 1000K and remains smooth thereafter. To seek a purely temperature induced change potentially around 1200K, we return to the screw dislocation calculations under zero-stress and finite temperatures from 600K to 1300K. For each temperature, the number of kps were counted and the dislocation location tracked over a long period. Since no mechanical stress is applied, these kps can be distinguished as thermal kink pairs (kps). As shown in Fig. 11, there is a dramatic increase in the number of thermal kps and the dislocation can glide forward without stress beyond 1200K. This finding suggests that when under stress, thermal kps can substantially assist in screw glide at T > 1200K.

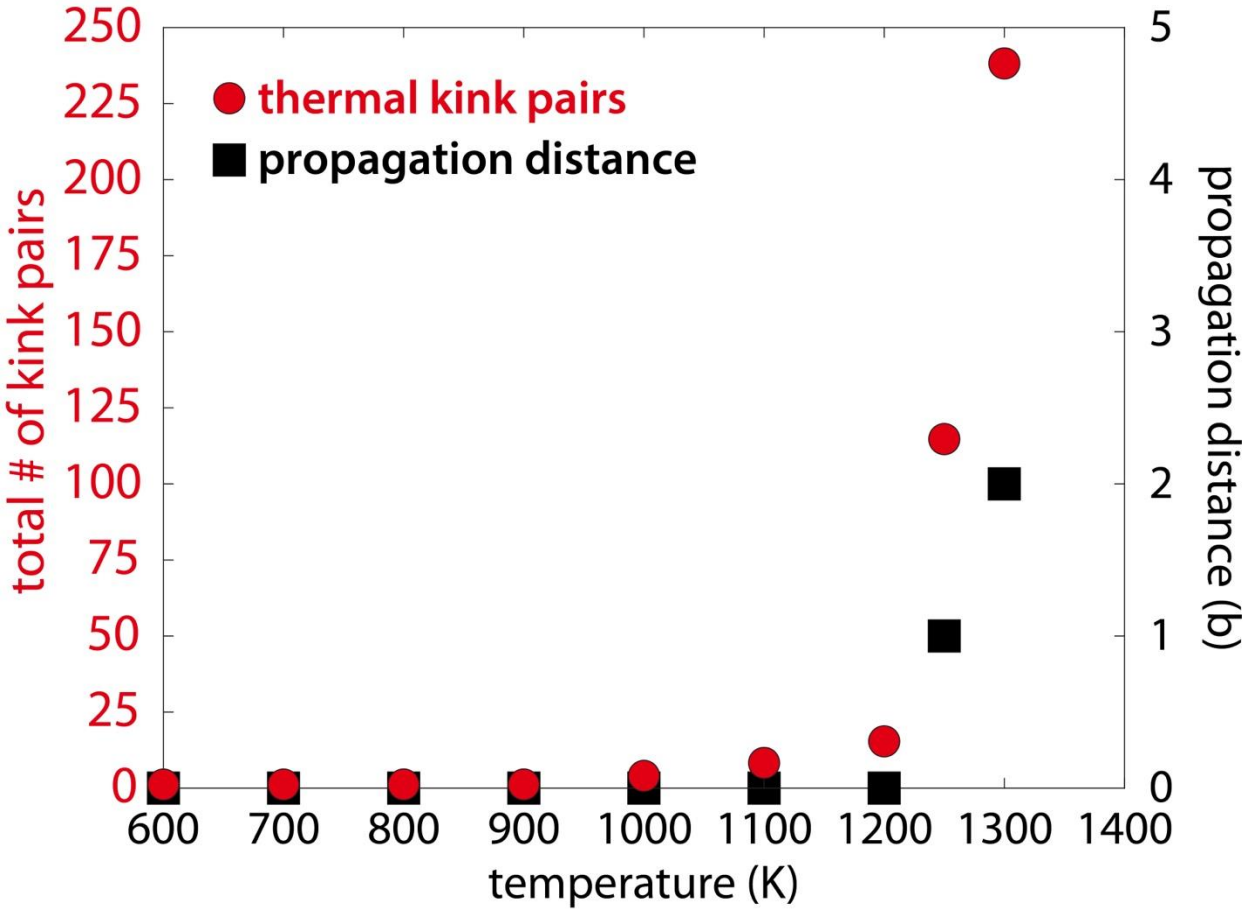

FIG. 11. *Total number of thermal kps and propagation distance plotted as a function of temperature at zero stress.*

Although the high-temperature material properties of RMPEAs are an area of active discussion, there are very few systematic studies to date that focus on the mechanistic origins of the strength plateau with respect to temperature. A recent study on dislocation glide in MoNbTi at 300K posited that dipole dragging may be responsible for the strength plateau between 900K–1200K [5]. This notion was based on the finding that there were numerous slip planes for glide in the MoNbTi

system. While our study focused on the (110) plane only, we do show evidence that the plateau is related to cross slip onto other {110} planes and formation of nonplanar kps. These nonplanar kps, once formed, however, do not migrate on the cross-slip plane and the adjacent segments of the dislocation continue to glide around these immobile nonplanar kps. This event would set itself up for dipole dragging, should vacancy formation and diffusion be included in the model formulation (which would be possible), and serve to further stabilize screw mobility against temperature.

It has also been proposed that the strength plateau can be explained by dynamic strain aging (DSA), whereby interstitials interact with edge dislocations and the stress to overcome these obstacles increases [7]. Recent PFDD calculations on pure refractories have shown that diffusing interstitials can pin edge dislocations and the higher their mobility, such as at high temperatures, the more likely can pin gliding dislocations [75]. While diffusing interstitials are not included here in simulation, the occasional exceptionally high USFE regions have a closely related pinning effect. It should be mentioned that DSA in traditional alloys is usually accompanied by other characteristics, such as a decrease in ductility and a negative strain rate sensitivity exponent [76]. In single-phase bcc RMPEAs, such as MoNbTaVW, however, experiments show that ductility remains high within the strength plateau region [17]. Additionally, studies on bcc RMPEAs have shown positive strain rate sensitivities [77].

Cross slip of short segments of a screw dislocation line in RMPEAs have been observed with both MD and kMC techniques. The intersection of two kinks on different glide planes forms a cross-kink, which has been shown to increase the stress required to move the screw dislocation [39]. For cross-kinking to occur, an edge segment of the kp must migrate some distance to eventually encounter another edge segment on a different glide plane, leading to the intersection. In kMC simulation on NbTaV, cross-kinking has been shown to be an effective strengthening mechanism up to 900K, after which cross-kink diffusion leads to their annihilation and rapid macroscopic softening [39]. The same phenomenon has been observed with MD simulations on NbTiZr, where cross-kink pinning awards high strength at low homologous temperatures [22]. Although current PFDD simulations would allow for cross-kinking, we did not see any evidence of it. Instead, temperature-induced nonplanar kps formation and their inability to expand caused screw glide resistance and mobility reduction. With strengthening via cross-kinking in screw dislocations predicted to cease at 900K, a later mesoscale kMC/DD study on MoNbTaW elected to focus attention on edge dislocations between 500K-2000K [15]. They showed that when using a thermally activated superjog model, superjogs can act as extra pinning points that increase the activation stress. An analytical model based on the simulation results was introduced that agrees reasonably well with the experimentally observed strength plateau from 900K-1500K. At the length and time scales of the present PFDD technique, superjog formation would require integrating vacancy formation and diffusion into the basic formulation, which is possible but neglected in the current application. It may be important for future simulations of edge dislocations in RMPEAs, leading to a reduction in edge mobility.

Conclusions

In summary, PFDD was used to investigate the high temperature glide mechanisms of edge and screw dislocations in the equiatomic MoNbTi RMPEA. From 600K–1200K, edge dislocations display smooth glide and an increase in glide distance with increasing temperature. Edge glide

mechanism does not change as a function of stress or temperature. Conversely, screw dislocations tend to exhibit jerky glide at lower stresses and/or temperatures. Above 1000K, the screw will begin to exhibit smooth glide. As temperature was increased from 600K to 1300K, three distinct screw glide mechanisms were observed, namely 1) multiple kp (kp) formation at low temperatures, 2) overlapping kp formation at medium temperatures, and 3) overlapping and nonplanar kp formation at higher temperatures. Nonplanar kp formation was found to inhibit screw glide and produced athermal, stress-independent mobility from 1100K−1200K, which coincides with the experimental yield strength plateau. Glide by thermal kp formation alone was detected in simulation at temperatures above 1200K, when softening in the yield stress is seen experimentally to begin. The results altogether suggest that in MoNbTi, screw dislocation motion contributes to observed changes in yield strength even in high temperature deformation.

Acknowledgments M. R. J. and I. J. B. gratefully acknowledge support from the Office of Naval Research under contract N00014-21-1-2536. M. R. J. acknowledges this paper was supported in part by a fellowship award under contract FA9550-21-F-0003 through the National Defense Science and Engineering Graduate (NDSEG) Fellowship Program, sponsored by the Air Force Research Laboratory (AFRL), the Office of Naval Research (ONR) and the Army Research Office (ARO). L. T. W. F. acknowledges support from the Department of Energy National Nuclear Security Administration Stewardship Science Graduate Fellowship, which is provided under cooperative agreement number DE-NA0003960. Use was made of computational facilities purchased with funds from the National Science Foundation (CNS-1725797) and administered by the Center for Scientific Computing (CSC). The CSC is supported by the California NanoSystems Institute and the Materials Research Science and Engineering Center (MRSEC; NSF DMR 2308708) at UC Santa Barbara.

References

[1] D. B. Miracle and O. N. Senkov, *A Critical Review of High Entropy Alloys and Related Concepts*, Acta Mater **122**, 448 (2017).

[2] E. P. George, D. Raabe, and R. O. Ritchie, *High-Entropy Alloys*, Nat Rev Mater **4**, 515 (2019).

[3] S. Dixit, S. Rodriguez, M. R. Jones, P. Buzby, R. Dixit, N. Argibay, F. W. DelRio, H. H. Lim, and D. Fleming, *Refractory High-Entropy Alloy Coatings for High-Temperature Aerospace and Energy Applications*, Journal of Thermal Spray Technology **31**, 1021 (2022).

[4] O. N. Senkov, D. B. Miracle, K. J. Chaput, and J.-P. Couzinie, *Development and Exploration of Refractory High Entropy Alloys—A Review*, J Mater Res **33**, 3092 (2018).

[5] F. Wang, G. H. Balbus, S. Xu, Y. Su, J. Shin, P. F. Rottmann, K. E. Knipling, J.-C. Stinville, L. H. Mills, and O. N. Senkov, *Multiplicity of Dislocation Pathways in a Refractory Multiprincipal Element Alloy*, Science (1979) **370**, 95 (2020).

[6] X. Liu, D. Hua, W. Wang, Q. Zhou, S. Li, J. Shi, Y. He, and H. Wang, *Atomistic Understanding of Incipient Plasticity in BCC Refractory High Entropy Alloys*, J Alloys Compd **920**, 166058 (2022).

[7] F. Maresca and W. A. Curtin, *Mechanistic Origin of High Strength in Refractory BCC High Entropy Alloys up to 1900K*, Acta Mater **182**, 235 (2020).

[8] S. Gorsse, M. H. Nguyen, O. N. Senkov, and D. B. Miracle, *Database on the Mechanical Properties of High Entropy Alloys and Complex Concentrated Alloys*, Data Brief **21**, 2664 (2018).
[9] X. Wang, F. Maresca, and P. Cao, *The Hierarchical Energy Landscape of Screw Dislocation Motion in Refractory High-Entropy Alloys*, Acta Mater **234**, 118022 (2022).
[10] Y. Tong, S. Zhao, H. Bei, T. Egami, Y. Zhang, and F. Zhang, *Severe Local Lattice Distortion in Zr-and/or Hf-Containing Refractory Multi-Principal Element Alloys*, Acta Mater **183**, 172 (2020).
[11] O. N. Senkov, S. v Senkova, D. B. Miracle, and C. Woodward, *Mechanical Properties of Low-Density, Refractory Multi-Principal Element Alloys of the Cr–Nb–Ti–V–Zr System*, Materials Science and Engineering: A **565**, 51 (2013).
[12] F. Maresca and W. A. Curtin, *Theory of Screw Dislocation Strengthening in Random BCC Alloys from Dilute to "High-Entropy" Alloys*, Acta Mater **182**, 144 (2020).
[13] S. Yin, Y. Zuo, A. Abu-Odeh, H. Zheng, X.-G. Li, J. Ding, S. P. Ong, M. Asta, and R. O. Ritchie, *Atomistic Simulations of Dislocation Mobility in Refractory High-Entropy Alloys and the Effect of Chemical Short-Range Order*, Nat Commun **12**, 4873 (2021).
[14] B. Chen, S. Li, H. Zong, X. Ding, J. Sun, and E. Ma, *Unusual Activated Processes Controlling Dislocation Motion in Body-Centered-Cubic High-Entropy Alloys*, Proceedings of the National Academy of Sciences **117**, 16199 (2020).
[15] S. He, X. Zhou, D. Mordehai, and J. Marian, *Thermal Super-Jogs Control the High-Temperature Strength Plateau in Nb-Mo-Ta-W Alloys*, Acta Mater **244**, 118539 (2023).
[16] R. R. Eleti, N. Stepanov, N. Yurchenko, S. Zherebtsov, and F. Maresca, *Cross-Kink Unpinning Controls the Medium- to High-Temperature Strength of Body-Centered Cubic NbTiZr Medium-Entropy Alloy*, Scr Mater **209**, 114367 (2022).
[17] O. N. Senkov, G. B. Wilks, J. M. Scott, and D. B. Miracle, *Mechanical Properties of Nb25Mo25Ta25W25 and V20Nb20Mo20Ta20W20 Refractory High Entropy Alloys*, Intermetallics (Barking) **19**, 698 (2011).
[18] H. Lim, C. C. Battaile, J. D. Carroll, B. L. Boyce, and C. R. Weinberger, *A Physically Based Model of Temperature and Strain Rate Dependent Yield in BCC Metals: Implementation into Crystal Plasticity*, J Mech Phys Solids **74**, 80 (2015).
[19] K.-K. Tseng, H.-H. Huang, W.-R. Wang, J.-W. Yeh, and C.-W. Tsai, *Edge-Dislocation-Induced Ultrahigh Elevated-Temperature Strength of HfMoNbTaW Refractory High-Entropy Alloys*, Sci Technol Adv Mater **23**, 642 (2022).
[20] O. N. Senkov, S. Gorsse, and D. B. Miracle, *High Temperature Strength of Refractory Complex Concentrated Alloys*, Acta Mater **175**, 394 (2019).
[21] S. I. Rao, C. Woodward, B. Akdim, O. N. Senkov, and D. Miracle, *Theory of Solid Solution Strengthening of BCC Chemically Complex Alloys*, Acta Mater **209**, 116758 (2021).
[22] F. Maresca and W. A. Curtin, *Theory of Screw Dislocation Strengthening in Random BCC Alloys from Dilute to "High-Entropy" Alloys*, Acta Mater **182**, 144 (2020).
[23] N. K. Aragon, S. Yin, H. Lim, and I. Ryu, *Temperature Dependent Plasticity in BCC Micropillars*, Materialia (Oxf) **19**, 101181 (2021).
[24] A. S. Schneider, D. Kaufmann, B. G. Clark, C. P. Frick, P. A. Gruber, R. Mönig, O. Kraft, and E. Arzt, *Correlation between Critical Temperature and Strength of Small-Scale Bcc Pillars*, Phys Rev Lett **103**, 105501 (2009).

[25] S. Takeuchi, T. Hashimoto, and K. Maeda, *Plastic Deformation of Bcc Metal Single Crystals at Very Low Temperatures*, Transactions of the Japan Institute of Metals **23**, 60 (1982).
[26] B. Šesták and A. Seeger, *The Relationship between the Work-Hardening of BCC and FCC Metals*, Physica Status Solidi (b) **43**, 433 (1971).
[27] C. Lee et al., *Temperature Dependence of Elastic and Plastic Deformation Behavior of a Refractory High-Entropy Alloy*, Sci Adv **6**, eaaz4748 (2022).
[28] L. Lilensten, J.-P. Couzinié, L. Perrière, A. Hocini, C. Keller, G. Dirras, and I. Guillot, *Study of a Bcc Multi-Principal Element Alloy: Tensile and Simple Shear Properties and Underlying Deformation Mechanisms*, Acta Mater **142**, 131 (2018).
[29] J.-Ph. Couzinié, L. Lilensten, Y. Champion, G. Dirras, L. Perrière, and I. Guillot, *On the Room Temperature Deformation Mechanisms of a TiZrHfNbTa Refractory High-Entropy Alloy*, Materials Science and Engineering: A **645**, 255 (2015).
[30] C. Lee et al., *Strength Can Be Controlled by Edge Dislocations in Refractory High-Entropy Alloys*, Nat Commun **12**, 5474 (2021).
[31] R. E. Kubilay, A. Ghafarollahi, F. Maresca, and W. A. Curtin, *High Energy Barriers for Edge Dislocation Motion in Body-Centered Cubic High Entropy Alloys*, NPJ Comput Mater **7**, 112 (2021).
[32] S. I. Rao, C. Varvenne, C. Woodward, T. A. Parthasarathy, D. Miracle, O. N. Senkov, and W. A. Curtin, *Atomistic Simulations of Dislocations in a Model BCC Multicomponent Concentrated Solid Solution Alloy*, Acta Mater **125**, 311 (2017).
[33] S. I. Rao, B. Akdim, E. Antillon, C. Woodward, T. A. Parthasarathy, and O. N. Senkov, *Modeling Solution Hardening in BCC Refractory Complex Concentrated Alloys: NbTiZr, Nb1. 5TiZr0. 5 and Nb0. 5TiZr1. 5*, Acta Mater **168**, 222 (2019).
[34] B. Chen, S. Li, J. Ding, X. Ding, J. Sun, and E. Ma, *Correlating Dislocation Mobility with Local Lattice Distortion in Refractory Multi-Principal Element Alloys*, Scr Mater **222**, 115048 (2023).
[35] N. Deka and R. B. Sills, *Monte Carlo-Discrete Dislocation Dynamics: A Technique for Studying the Formation and Evolution of Dislocation Structures*, Model Simul Mat Sci Eng **30**, 024002 (2021).
[36] A. Zhu, C. Jin, D. Zhao, Y. Xiang, and J. Huang, *A Numerical Scheme for Generalized Peierls-Nabarro Model of Dislocations Based on the Fast Multipole Method and Iterative Grid Redistribution*, Commun Comput Phys **18**, 1282 (2015).
[37] K. Lin and D. C. Chrzan, *Kinetic Monte Carlo Simulation of Dislocation Dynamics*, Phys Rev B **60**, 3799 (1999).
[38] I. J. Beyerlein and A. Hunter, *Understanding Dislocation Mechanics at the Mesoscale Using Phase Field Dislocation Dynamics*, Philosophical Transactions of the Royal Society A: Mathematical, Physical and Engineering Sciences **374**, 20150166 (2016).
[39] X. Zhou, S. He, and J. Marian, *Cross-Kinks Control Screw Dislocation Strength in Equiatomic Bcc Refractory Alloys*, Acta Mater **211**, 116875 (2021).
[40] S. Xu, Y. Su, L. T. W. Smith, and I. J. Beyerlein, *Frank-Read Source Operation in Six Body-Centered Cubic Refractory Metals*, J Mech Phys Solids **141**, 104017 (2020).
[41] L. T. W. Smith, Y. Su, S. Xu, A. Hunter, and I. J. Beyerlein, *The Effect of Local Chemical Ordering on Frank-Read Source Activation in a Refractory Multi-Principal Element Alloy*, Int J Plast **134**, 102850 (2020).

[42] L. T. W. Fey, A. Hunter, and I. J. Beyerlein, *Phase-Field Dislocation Modeling of Cross-Slip*, J Mater Sci (2022).
[43] C. Albrecht, A. Hunter, A. Kumar, and I. J. Beyerlein, *A Phase Field Model for Dislocations in Hexagonal Close Packed Crystals*, J Mech Phys Solids **137**, 103823 (2020).
[44] X. Peng, N. Mathew, I. J. Beyerlein, K. Dayal, and A. Hunter, *A 3D Phase Field Dislocation Dynamics Model for Body-Centered Cubic Crystals*, Comput Mater Sci **171**, 109217 (2020).
[45] L. T. W. Fey, S. Xu, Y. Su, A. Hunter, and I. J. Beyerlein, *Transitions in the Morphology and Critical Stresses of Gliding Dislocations in Multiprincipal Element Alloys*, Phys Rev Mater **6**, 013605 (2022).
[46] H. Zheng, L. T. W. Fey, X.-G. Li, Y.-J. Hu, L. Qi, C. Chen, S. Xu, I. J. Beyerlein, and S. P. Ong, *Multi-Scale Investigation of Short-Range Order and Dislocation Glide in MoNbTi and TaNbTi Multi-Principal Element Alloys*, NPJ Comput Mater **9**, 89 (2023).
[47] C. Albrecht, I. J. Beyerlein, and M. R. Jones, *Temperature Dependent Phase Field Dislocation Dynamics Model*, European Journal of Mechanics - A/Solids **100**, 104987 (2023).
[48] X. Wang, S. Xu, W.-R. Jian, X.-G. Li, Y. Su, and I. J. Beyerlein, *Generalized Stacking Fault Energies and Peierls Stresses in Refractory Body-Centered Cubic Metals from Machine Learning-Based Interatomic Potentials*, Comput Mater Sci **192**, 110364 (2021).
[49] C. Yang and L. Qi, *Modified Embedded-Atom Method Potential of Niobium for Studies on Mechanical Properties*, Comput Mater Sci **161**, 351 (2019).
[50] X. Zhang, J. Tang, L. Deng, G. Zhong, X. Liu, Y. Li, H. Deng, and W. Hu, *The Effects of Interstitial Impurities on the Mechanical Properties of Vanadium Alloys: A First-Principles Study*, J Alloys Compd **701**, 975 (2017).
[51] S. L. Frederiksen and K. W. Jacobsen, *Density Functional Theory Studies of Screw Dislocation Core Structures in Bcc Metals*, Philosophical Magazine **83**, 365 (2003).
[52] L. H. Yang, P. Söderlind, and J. A. Moriarty, *Accurate Atomistic Simulation of (a/2)〈111〉 Screw Dislocations and Other Defects in Bcc Tantalum*, Philosophical Magazine A **81**, 1355 (2001).
[53] K. Kawasaki, *Simple Derivations of Generalized Linear and Nonlinear Langevin Equations*, Journal of Physics A: Mathematical, Nuclear and General **6**, 1289 (1973).
[54] T. Ichitsubo and K. Tanaka, *Thermal Fluctuation for the Time-Dependent Ginzburg-Landau Simulation*, Phys Rev E **63**, 060101 (2001).
[55] L. D. Landau and E. M. Lifshitz, *Chapter i–the Fundamental Principles of Statistical Physics*, Course of Theoretical Physics 1 (1980).
[56] *See Supplemental Material at [Link] for a Description of DFT Methodology.*
[57] S. Xu, E. Hwang, W.-R. Jian, Y. Su, and I. J. Beyerlein, *Atomistic Calculations of the Generalized Stacking Fault Energies in Two Refractory Multi-Principal Element Alloys*, Intermetallics (Barking) **124**, 106844 (2020).
[58] A. Zunger, S.-H. Wei, L. G. Ferreira, and J. E. Bernard, *Special Quasirandom Structures*, Phys Rev Lett **65**, 353 (1990).
[59] A. Van de Walle, P. Tiwary, M. De Jong, D. L. Olmsted, M. Asta, A. Dick, D. Shin, Y. Wang, L.-Q. Chen, and Z.-K. Liu, *Efficient Stochastic Generation of Special Quasirandom Structures*, Calphad **42**, 13 (2013).

[60] G. Kresse and J. Furthmüller, *Efficient Iterative Schemes for Ab Initio Total-Energy Calculations Using a Plane-Wave Basis Set*, Phys Rev B **54**, 11169 (1996).
[61] G. Kresse and D. Joubert, *From Ultrasoft Pseudopotentials to the Projector Augmented-Wave Method*, Phys Rev B **59**, 1758 (1999).
[62] P. E. Blöchl, *Projector Augmented-Wave Method*, Phys Rev B **50**, 17953 (1994).
[63] J. P. Perdew, K. Burke, and M. Ernzerhof, *Generalized Gradient Approximation Made Simple*, Phys Rev Lett **77**, 3865 (1996).
[64] H. J. Monkhorst and J. D. Pack, *Special Points for Brillouin-Zone Integrations*, Phys Rev B **13**, 5188 (1976).
[65] M. Methfessel and A. T. Paxton, *High-Precision Sampling for Brillouin-Zone Integration in Metals*, Phys Rev B **40**, 3616 (1989).
[66] S. H. Zhang and R. F. Zhang, *AELAS: Automatic ELAStic Property Derivations via High-Throughput First-Principles Computation*, Comput Phys Commun **220**, 403 (2017).
[67] G. Laplanche, P. Gadaud, L. Perrière, I. Guillot, and J. P. Couzinié, *Temperature Dependence of Elastic Moduli in a Refractory HfNbTaTiZr High-Entropy Alloy*, J Alloys Compd **799**, 538 (2019).
[68] *Phonon Density of States of the Debye Model*, (unpublished).
[69] S. Xu, W.-R. Jian, Y. Su, and I. J. Beyerlein, *Line-Length-Dependent Dislocation Glide in Refractory Multi-Principal Element Alloys*, Appl Phys Lett **120**, (2022).
[70] L. T. W. Fey and I. J. Beyerlein, *Random Generation of Lattice Structures with Short-Range Order*, Integr Mater Manuf Innov **11**, 382 (2022).
[71] H. Zheng, L. T. W. Fey, X.-G. Li, Y.-J. Hu, L. Qi, C. Chen, S. Xu, I. J. Beyerlein, and S. P. Ong, *Multi-Scale Investigation of Chemical Short-Range Order and Dislocation Glide in the MoNbTi and TaNbTi Refractory Multi-Principal Element Alloys*, ArXiv Preprint ArXiv:2203.03767 (2022).
[72] J. P. Hirth, J. Lothe, and T. Mura, *Theory of Dislocations*, J Appl Mech **50**, 476 (1983).
[73] S. Xu, Y. Su, W.-R. Jian, and I. J. Beyerlein, *Local Slip Resistances in Equal-Molar MoNbTi Multi-Principal Element Alloy*, Acta Mater **202**, 68 (2021).
[74] Q.-J. Li, H. Sheng, and E. Ma, *Strengthening in Multi-Principal Element Alloys with Local-Chemical-Order Roughened Dislocation Pathways*, Nat Commun **10**, 3563 (2019).
[75] L. T. W. Fey, C. Reynolds, A. Hunter, and I. J. Beyerlein, *Phase-Field Modeling of Dislocation–Interstitial Interactions*, J Mech Phys Solids **179**, 105370 (2023).
[76] A. Van den Beukel and U. F. Kocks, *The Strain Dependence of Static and Dynamic Strain-Aging*, Acta Metallurgica **30**, 1027 (1982).
[77] M. A. Melia, S. R. Whetten, R. Puckett, M. Jones, M. J. Heiden, N. Argibay, and A. B. Kustas, *High-Throughput Additive Manufacturing and Characterization of Refractory High Entropy Alloys*, Appl Mater Today **19**, 100560 (2020).